Transonic Study of Active Flutter Suppression Based on an Energy Concept

Maynard C. Sandford,* Irving Abel,† and David L. Gray‡
NASA Langley Research Center, Hampton, Va.

The application of active control technology to the suppression of flutter has been successfully demonstrated in the Langley transonic dynamics tunnel. This study involved the implementation of an aerodynamic-energy criterion to suppress flutter of a simplified delta-wing model. Use of this technique with both leading- and trailing-edge active controls has resulted in an increase in dynamic pressure of 22% above the basic wing flutter point and with only a trailing-edge active control has resulted in an increase in dynamic pressure of 30% above the basic wing flutter point at a Mach number of 0.9. Analytical methods used to predict the open- and closed-loop behavior of the model are also discussed.

Nomenclature

b	= reference semichord
b_m	= one-half mean geometric chord of wing
c	= reference chord, $2b$
$h(x,y,t)$	= vertical displacement
h_1, h_2	= vertical displacement of model at 30% and 70% of the reference chord, respectively (Fig. 5)
M_i	= generalized mass of ith vibration mode
m	= total mass of wing model, includes semispan wing and nacelles
$m(x,y)$	= mass distribution
$\Delta p(x,y,t)$	= pressure distribution
q_i	= generalized displacement of ith vibration mode
S	= reference area
s	= laplace operator
t	= time
U	= aerodynamic-energy matrix defined in Eq. (2)
$\bar{U}$	= complex conjugate of the matrix U
V	= freestream velocity
v	= volume of a conical frustum having wing root chord as base diameter, wing tip chord as upper diameter, and wing semispan as height
x,y	= streamwise and spanwise coordinates, respectively
$Z_i(x,y)$	= normalized deflection in ith vibration mode
μ	= mass-density ratio, m/(test medium density) $\times (v)$
α	= angle of attack at Sec. A-A (Fig. 5)
β	= leading-edge-control deflection
δ	= trailing-edge-control deflection
$\delta_{t,c}$	= deflection command signal to trailing-edge control
ω	= circular frequency
ω_2	= circular frequency of second structural vibration mode
$\{\ \}$	= column matrix
$\lfloor\ \rfloor$	= row matrix
$[\ ]$	= square matrix
$[\ ]^T$	= transpose of matrix

Presented as Paper 74-403 at the AIAA/ASME/SAE 15th Structures, Structural Dynamics and Materials Conference, Las Vegas, Nevada, April 17-19, 1974; submitted May 6, 1974; revision received September 30, 1974.

Index categories: Aeroelasticity and Hydroelasticity.

*Aerospace Engineer, Aeroelasticity Branch. Member AIAA.
†Aerospace Engineer, Aeroelasticity Branch.
‡Aerospace Engineer, Electro-Mechanical Instrumentation Branch.

§Dots above symbols indicate derivatives with respect to time.

Introduction

CURRENTLY, there is considerable interest in the use of active control technology for flutter suppression and application of this technology appears to have the potential for reducing aircraft structural weight. A method for flutter suppression using active controls proposed by E. Nissim[1] is based on aerodynamic energy considerations. This approach states that a sufficient condition for flutter prevention is that for all oscillatory motions of an elastic system in an airstream (i.e., an aircraft wing) positive work must be done by the system on the surrounding airstream. By appropriately equipping an elastic system with aerodynamic control surfaces which are related to motions of the system by a "control law" it is theoretically possible to increase the flutter speed of the system. Since this energy approach to flutter suppression appears promising, a wind-tunnel model program was initiated at the NASA Langley Research Center to experimentally evaluate this method. The purpose of this paper is to present the significant results of this model study. (Some early progress on this study is reported in Refs. 2 and 3).

The wind-tunnel model used for the flutter suppression program is a simplified version of a proposed supersonic transport wing design. The 1/17-size semispan model was an aspect ratio 1.28 cropped delta with a 50.5° leading-edge sweepback angle. The model was equipped with an active flutter suppression system consisting of hydraulically operated leading- and trailing-edge control surfaces located at about the 80% span of the wing. Each control surface was actuated by feedback signals from two accelerometers which monitor the wing surface motion.

This model was used to experimentally evaluate three control laws that were derived from aerodynamic energy considerations. The first two control laws used both the leading-edge and trailing-edge control surfaces. The third control law used only the trailing-edge control surface.

Experimental flutter data were obtained in the Langley transonic dynamics tunnel at Mach numbers of 0.6, 0.7, 0.8, and 0.9. Results for both the flutter suppression system operating (closed-loop) and not operating (open-loop) were obtained. These data were correlated with analytical flutter calculations based on doublet lattice aerodynamics and experimentally determined mode shapes, generalized masses, and natural frequencies for the first nine wing modes.

Flutter Suppression Based on Aerodynamic Energy Considerations

Flutter is a self-excited oscillation in which energy is absorbed by the lifting surface from the airstream. The state of stability of the system is defined by the sign of the work per cycle when the lifting surface undergoes an arbitrary oscillatory motion. The use of energy techniques to in-

vestigate the stability of an aeroelastic system is not new[4]; however, a recent contribution to the area of flutter suppression is the development of an aerodynamic energy criterion by Nissim.[1] This criterion states that a necessary and sufficient condition for the prevention of flutter is that for all allowable oscillatory motions of an elastic system in an airstream, positive work must be done by the system on the surrounding airstream. A brief summary of the salient points brought out in Ref. 1 is given in the following section.

Energy Concept

Consider the equations of motion for a system with n degrees of freedom:

$$\{F\} = -\omega^2 \left[[M] + \pi\rho b^4 S[[A_R] + i[A_I]] \right] \{q\} + [K]\{q\} \quad (1)$$

where, at flutter, the generalized force $\{F\} = 0$ and ω is the circular frequency of oscillation; $[M]$ is the mass matrix (called B in Ref. 1); $[A_R]$ and $[A_I]$ are the real and imaginary unsteady aerodynamic-force matrices, respectively; $[K]$ is the structural stiffness matrix (called E in Ref. 1); ρ is the fluid density; S and b are a reference area and length, respectively; and $\{q\}$ is the generalized displacement vector.

Nissim shows that the work per cycle W (called P in Ref. 1) done by the system on the airstream can be written as

$$W = \frac{1}{2} \pi^2 \rho b^4 S \omega^2 \lfloor q_R - iq_I \rfloor [U] \{q_R + iq_I\} \quad (2)$$

where

$$\{q\} = \{q_R + iq_I\} e^{i\omega t}$$

and

$$[U] = \left[-[[A_I] + [A_I]^T] + i[[A_R] - [A_R]^T] \right]$$

A positive value for W indicates a transfer of energy from the system to the airstream, and hence stability. The maxtrix U is Hermitian (i.e., $\bar{U}^T = U$) and therefore possesses real eigenvalues. By use of these eigenvalues it is shown in Ref. 1 that the energy input per cycle into the airstream can be reduced to a principal quadratic form as

$$W = \frac{1}{2} \pi^2 \rho b^4 \omega^2 S[\lambda_1 (\xi_{R_1}^2 + \xi_{I_1}^2) + \lambda_2 (\xi_{R_2}^2 + \xi_{I_2}^2) + \ldots + \lambda_n (\xi_{R_n}^2 + \xi_{I_n}^2)] \quad (3)$$

where $\lambda_1, \lambda_2, \ldots, \lambda_n$ are the eigenvalues of the matrix U and ξ denotes generalized coordinates associated with the aerodynamic energy. It can be seen from Eq. (3) that the work W will always be positive if all the eigenvalues λ are positive. Therefore, a sufficient condition for flutter stability is that all the λ terms are positive. A notable characteristic of the energy method is that the criterion for flutter stability is determined by the characteristics of the aerodynamic-force matrices alone. Therefore, if a particular system has undesirable flutter characteristics (i.e., too low a flutter speed), the flutter characteristics can be improved if a mechanism can be found which changes the U matrix in an appropriate manner. One such mechanism is the addition of control surfaces to the basic system. The motions of these surfaces generate aerodynamic forces which modify the aerodynamic terms in the U matrix for the basic system. For flutter suppression the control-surface deflections are related by a "control law" to the plunging and pitching motion of the main surface. Nissim points out in Ref. 1 that a suitable configuration is one employing both leading- and trailing-edge controls since the two working together provide independent control of lift and pitching moment.

Delta-Wing Flutter Suppression Model

To evaluate the practical aspects of the aerodynamic-energy concept, The Boeing Company, Wichita Division, under contract to NASA, performed an analytical study of the application of this concept to an early supersonic transport (SST) configuration. Some results of this study, as described in Ref. 5, indicate increases in the flutter speed from 11% to 29% for several spanwise locations of leading- and trailing-edge controls. Because of these positive results, an experimental program aimed at providing evaluation and validation of the energy concept was initiated by using a wall-mounted 1/17-size simplified semispan model of a recent SST configuration. The Boeing Company, under contract to the Langley Research Center, is providing general support for this program in the area of controls implementation and analysis. A photograph of the model installed in the Langley transonic dynamics tunnel is shown in Fig. 1, and a sketch of the model is presented in Fig. 2.

The wing has a cropped-delta planform without twist or camber, a symmetric circular-art airfoil section with a maximum thickness-to-chord ratio of 0.03, and hydraulically actuated leading- and trailing-edge controls. The trailing-edge control was approximately 20% of the local chord, while the leading-edge control varied from about 15% of the chord inboard to 20% of the local chord outboard. Both controls were located between 73% and 84% of the wing span. These locations are approximately those referred to in Ref. 5 that resulted in the largest increase in flutter speed. Simulated engine nacelles are mounted on the underside of the wing. The model construction consists of an internal aluminum alloy plate that was tapered in thickness in the spanwise direction

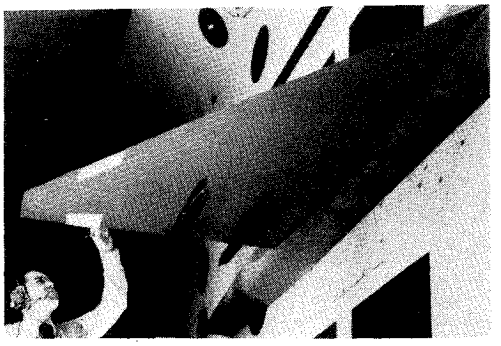

Fig. 1 Delta-wing flutter-suppression model.

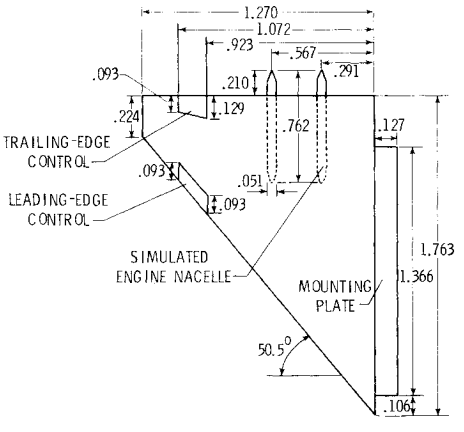

Fig. 2 Sketch of delta-wing. (All linear dimensions are in meters.)

and had cutouts to simulate spars and ribs. The plate was covered with balsa wood to provide the proper aerodynamic contour.

Because of the large hinge moments required and the necessity of keeping the control-surface actuation system within the physical constraints imposed by the model, that is, small and light, it was necessary to design and fabricate an electrohydraulic actuation system. Within these constraints an actuator was designed that weighs only 56.7 grams yet can produce approximately 4.52 $N-m$ of torque throughout the operating range of interest (approximately from 0 to 25 Hz). Because of the limited thickness of the wing, it was also necessary to design and fabricate special control-surface position indicators. This was accomplished by mounting silicon solar cells to the actuator control shaft and illuminating them with a stationary light source. As the control shaft rotates, a voltage proportional to the angular position of the surface is produced. A photograph of the model showing the actuator and position indicator is presented in Fig. 3. A complete description of the design and fabrication of the control actuation system for the model is given in Ref. 6.

To perform analytical calculations for the model, it was necessary to specify a set of generalized masses, mode shapes, and natural frequencies. These properties were determined experimentally for the first nine structural modes of the model by using methods similar to those described in Ref. 7. The measured mode shapes, natural frequencies, and generalized masses are given in Fig. 4.

Control Law

A simplified block diagram of the delta-wing flutter suppression system is presented in Fig. 5. The basic control law which relates control surface deflections to wing motion is of the form

$$\begin{Bmatrix}\beta\\ \delta\end{Bmatrix} = \begin{bmatrix} C_{11} & C_{12}\\ C_{21} & C_{22}\end{bmatrix}\begin{Bmatrix} h_1/b\\ \alpha\end{Bmatrix} + i\begin{bmatrix} G_{11} & G_{12}\\ G_{21} & G_{22}\end{bmatrix}\begin{Bmatrix} h_1/b\\ \alpha\end{Bmatrix} \quad (4)$$

where β is the leading-edge control surface deflection; δ is the trailing-edge control surface deflection; h_1 and α are the plunging and pitching motions, respectively, of a representative streamwise section of the wing (Sec $A-A$ in Fig. 5); b is a reference length; and C and G are constant coefficients which were determined by using the aerodynamic-energy concept.

The wing motion at h_1 and h_2 (see Fig. 5) locations are measured by linear accelerometers located at about 30% and 70% of the local chord c. The control law is mechanized on an analog computer which has been programed to perform the operations indicated in Fig. 5 to determine h_1 $\dot{h}_1$ α, and $\dot{\alpha}$, and pass the proper command signal as expressed in Eq. (4) to the control surfaces. Figure 5 indicates that the period of oscillation $1/\omega$ must be determined. A period measuring circuit was developed to obtain the term $1/\omega$ and was used throughout this study. Reference 1 showed that essentially the same results can be obtained if the value of $1/\omega$ is taken to be constant and equal to the open-loop flutter period. The present study confirmed by wind-tunnel tests that identical results were obtained by using either the period measuring circuit or a constant value (equal to the flutter period) to obtain the $1/\omega$ term.

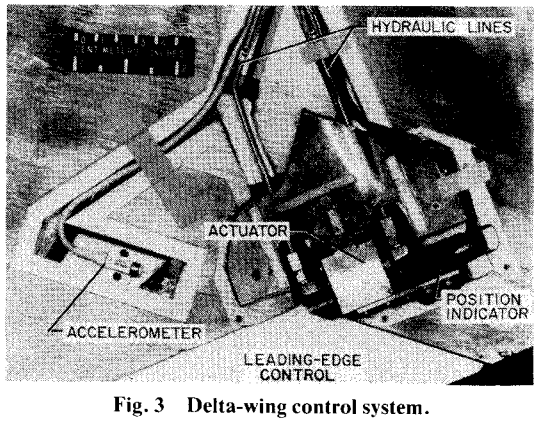

Fig. 3 Delta-wing control system.

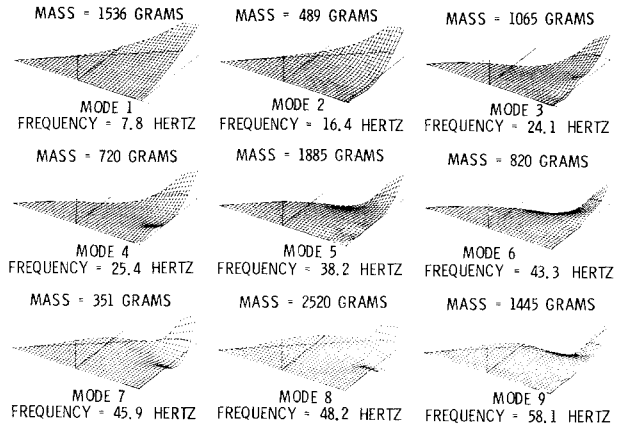

Fig. 4 Measured mode shapes, generalized masses, and frequencies of natural vibrational modes.

The three variations of the basic control law investigated in these studies were as follows:

Control Law A

$$\begin{Bmatrix}\beta\\ \delta\end{Bmatrix} = \begin{bmatrix} 0 & 5.6\\ 0 & -1.4\end{bmatrix}\begin{Bmatrix} h_1/b\\ \alpha\end{Bmatrix} + i\begin{bmatrix} 0 & 1.5\\ 0.6 & 0.2\end{bmatrix}\begin{Bmatrix} h_1/b\\ \alpha\end{Bmatrix}$$

Control Law B

$$\begin{Bmatrix}\beta\\ \delta\end{Bmatrix} = \begin{bmatrix} 0 & 0\\ 2.7 & -5.3\end{bmatrix}\begin{Bmatrix} h_1/b\\ \alpha\end{Bmatrix} + i\begin{bmatrix} 0 & 2.5\\ 1.0 & 0.75\end{bmatrix}\begin{Bmatrix} h_1/b\\ \alpha\end{Bmatrix}$$

Control Law C

$$\begin{Bmatrix}\beta\\ \delta\end{Bmatrix} = \begin{bmatrix} 0 & 0\\ 2.7 & -5.3\end{bmatrix}\begin{Bmatrix} h_1/b\\ \alpha\end{Bmatrix} + i\begin{bmatrix} 0 & 0\\ 2.5 & 0.75\end{bmatrix}\begin{Bmatrix} h_1 b\\ \alpha\end{Bmatrix}$$

Control Laws A and B require both a leading- and trailing-edge control surface. Whereas, Control Law C requires only a trailing-edge control surface. Control Law A was obtained from Ref. 1 where the derivation of the control law was based on two-dimensional unsteady aerodynamic theory. Therefore, as a first step Control Law A was used to experimentally evaluate the energy concept to the suppression of flutter. The next step in the flutter suppression study was to develop a control law by using three-dimensional unsteady theory. This resulted in the determination of a new set of $[C]$ and $[G]$ values (Control Law B). The final step in this study was to determine just how much benefit could be obtained from a trailing-edge control surface alone. With the three-

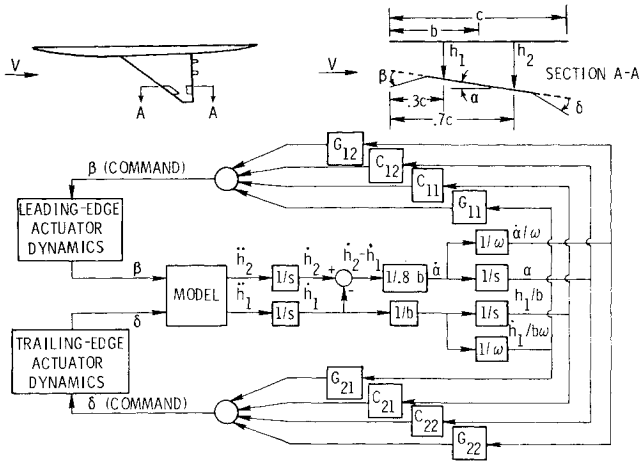

Fig. 5 Block diagram of flutter-suppression system.

dimensional aerodynamic-energy analysis, a trailing-edge control law was derived (Control Law C). It should be pointed out that the $[G]$ values shown for Control Laws B and C are compromised values from those of the analysis due to a dynamic instability of the control system. In effect, the using of the analytical values for $[G]$ resulted in a system that was so sensitive that if the model was disturbed in still air the control surfaces would begin to oscillate and support the disturbance. This problem is believed to be due to inertia coupling between the wing and the control surface.

Flutter Analysis

To illustrate the mechanism of flutter suppression, a flutter analysis, both with and without active controls, is presented. The flutter equations for a three-dimensional lifting surface are obtained from Lagrange's equation of motion by assuming that the unknown mode of motion is described by a linear combination of orthogonal modes, that is, the undamped natural modes of the system, in the following manner:

$$h(x,y,t)=\sum_{i=1}^{n} q_i(t)Z_i(x,y) \tag{5}$$

If structural damping is neglected, then the equations of motion become

$$M_i\ddot{q}_i(t)+\omega_i^2 M_i q_i(t)=Q_i(t) \tag{6}$$

where

$$M_i=\int_S\int m(x,y)Z_i^2(x,y)dx\,dy$$

is the generalized mass and

$$Q_i(t)=\int_S\int \Delta p(x,y,t)Z_i(x,y)dx\,dy$$

is the generalized aerodynamic force. The total pressure distribution $\Delta p(x,y,t)$ is composed of contributions due to each flexible mode plus those due to the leading- and trailing-edge controls. Therefore,

$$\Delta p(x,y,t)=\sum_{j=1}^{n}\Delta p_j(x,y)q_j(t)+\Delta p_\delta\delta+\Delta p_\beta\beta$$

where Δp_j is the pressure distribution due to each flexible mode, and Δp_β and Δp_δ are the pressure distributions due to leading- and trailing-edge controls, respectively. Substituting this expression for the pressures into Eq. (6) and expanding results in the following form of the equations of motion:

$$\begin{aligned}(-\omega^2M_i+\omega_i^2M_i)q_i(t)=&\\ \sum_{j=1}^{n}(q_j(t)\int_S\int\Delta p_jZ_i\,dx\,dy)+&\\ \beta\int_S\int\Delta p_\beta Z_i\,dx\,dy+&\\ \delta\int_S\int\Delta p_\delta Z_i\,dx\,dy&\end{aligned} \tag{7}$$

From Eq. (5), the nondimensionalized deflection of the wing for the responses h_1 and h_2 can be written as

$$\frac{h_1}{b}=\frac{1}{b}\sum_{i=1}^{n}q_i(t)Z_i(x_1,y_1)$$

$$\frac{h_2}{b}=\frac{1}{b}\sum_{i=1}^{n}q_i(t)Z_i(x_2,y_2)$$

Assuming that a straight line between the locations of the two sensors gives a reasonable approximation to the angle of attack at the reference station and noting that the sensors are $0.8b$ apart lead to the following equation for angle-of-attack:

$$\alpha=\frac{1}{0.8}\left(\frac{h_2}{b}-\frac{h_1}{b}\right)=\frac{1}{0.8b}\sum_{i=1}^{n}(Z_i(x_2,y_2)-Z_i(x_1,y_1))q_i(t)$$

Substituting the previous results into the control law (Eq. (4)) results in a matrix equation relating the control-surface motions to the generalized coordinates in the following form:

$$\begin{Bmatrix}\beta\\ \delta\end{Bmatrix}+\begin{bmatrix}A_1+iB_1 & A_2+iB_2 & \cdots & A_n+iB_n\\ C_1+iD_1 & C_2+iD_2 & \cdots & C_n+iD_n\end{bmatrix}\begin{Bmatrix}q_1\\ q_2\\ \vdots\\ q_n\end{Bmatrix} \tag{8}$$

where the parameters A_i, B_i, C_i, and D_i are constant coefficients defined as follows:

$$A_i=Z_i(x_1,y_1)\left(\frac{C_{11}}{b}-\frac{C_{12}}{0.8b}\right)+Z_i(x_2,y_2)\frac{C_{12}}{0.8b}$$

$$B_i=Z_i(x_1,y_1)\left(\frac{G_{11}}{b}-\frac{G_{12}}{0.8b}\right)+Z_i(x_2,y_2)\frac{G_{12}}{0.8b}$$

$$C_i=Z_i(x_1,y_1)\left(\frac{C_{21}}{b}-\frac{C_{22}}{0.8b}\right)+Z_i(x_2,y_2)\frac{C_{22}}{0.8b}$$

$$D_i=Z_i(x_1,y_1)\left(\frac{G_{21}}{b}-\frac{G_{22}}{0.8b}\right)+Z_i(x_2,y_2)\frac{G_{22}}{0.8b}$$

Substituting Eq. (8) into Eq. (7) results in the final form of the equations of motion:

$$\begin{aligned}(-\omega^2M_i+\omega_i^2M_i)q_i(t)=\sum_{j=1}^{n}q_j(&\int_S\int\Delta p_jZ_i\,dx\,dy\\ &+(A_j+iB_j)\int_S\int\Delta p_\beta Z_i\,dx\,dy\\ &+(C_j+iD_j)\int_S\int\Delta p_\delta Z_i\,dx\,dy)\end{aligned} \tag{9}$$

It should be noted from the form of the equations presented here that the active controls serve only to modify the aerodynamic forces of the wing alone. The Hermitian matrix U described earlier can be derived directly from the aerodynamic terms appearing in this equation and the effect of active controls on this matrix determined. Flutter calculations without active controls are performed by setting the coefficients A, B, C, and D equal to zero.

Flutter calculations were performed for the delta-wing model at Mach numbers of 0.6, 0.7, 0.8, and 0.9. The generalized aerodynamic forces appearing in Eq. (9) were formulated through the use of doublet-lattice aerodynamics as described in Ref. 8. This method requires the subdivision of the lifting surface into an array of trapezoidal boxes arranged in streamwise columns with a line of pulsating doublets located at the quarter chord of each box. The geometric boundary condition of tangential flow is satisfied at the 3/4-chord location for each box. The delta-wing model was divided into 160 boxes arranged in 16 streamwise strips with 10 boxes per strip. This arrangement provided six boxes on each control surface. All flutter calculations were made using the first nine measured structural modes, generalized masses, and natural frequencies. It should be noted that the equations of motion did not include control-surface dynamics since the natural frequency of rotation for each surface was considerably above the frequency of interest.

Discussion of Results

General

These flutter studies were conducted in the Langley transonic dynamics tunnel at Mach numbers of 0.6, 0.7, 0.8, and 0.9. For the basic wing (open-loop) flutter the control surfaces were kept at 0° deflection by applying hydraulic pressure to the actuators. The pressurized system provided each control surface with a very stiff spring and resulted in rotational frequencies of the controls many times higher than the wing flutter frequency. The open-loop flutter boundary of the model was established first, then an evaluation of the effect of active controls (closed-loop) on raising the boundary was begun. Included in these studies were evaluation of Control Laws A, B, and C. All closed-loop studies of Control Laws A and B were restricted to a Mach number of 0.9 because of an unexplained high-frequency, large-amplitude oscillation of the leading-edge control surface. This phenomenon occurred around 65 Hz, whereas the flutter frequencies were 11 to 12.5 Hz. The problem is not believed to be a result of the control law, since this motion to a lesser degree is also observed with the control loop open, but is introduced in some manner by the mechanization of the controls on the model.

By use of high-speed motion pictures and visual observation it was determined that the flutter motion of the wing model for both open-loop and closed-loop operation was similar in nature and closely resembled the second natural vibration mode coupled with some primary bending.

Experimental and Analytical

A comparison of calculated and experimental results showing the effect of each control law on raising the open-loop flutter boundary is presented in Fig. 6. The results are presented in terms of percent increase in dynamic pressure at $M=0.9$. By using Control Law A a 12% increase in dynamic pressure was obtained. The calculated increase for Control Law A is in excellent agreement with the experimental values. An earlier analytical treatment for this control law was reported in Ref. 3 and showed a 21% increase in the flutter dynamic pressure. The differences between theory and experiment in Ref. 3 were attributed in part to the instability of the aerodynamic theory to adequately predict control surface pressure distributions. Early in the design of the delta-wing model static hinge-moment measurements were made to aid in

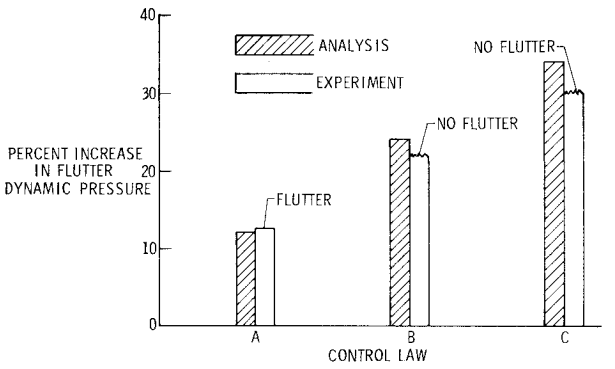

Fig. 6 Effect of different control laws on flutter dynamic pressure at $M=0.9$.

the design of the control actuators. It is shown in Ref. 2 that the calculated values of hinge moment are somewhat higher than those that were measured. For the present analytical investigation the theoretical unsteady aerodynamic forces for the leading and trailing edge control surfaces were adjusted to take into account the differences between measured and calculated static hinge moments. The analytical results for Control Law B indicate a predicted increase of 24%. The experimental results demonstrate a minimum increase of 22%. Experimental results for Control Law B do not represent a closed-loop flutter point since further increase in dynamic pressure were restricted by the high-frequency oscillation of the leading-edge control surface mentioned earlier. Of the three control laws investigated, the largest increase in flutter dynamic pressure was obtained with Control Law C. A minimum increase in dynamic pressure of 30% was obtained with this control law. The model was not tested to closed-loop flutter condition since the goal for these tests was set at a 30% increase in dynamic pressure assuming that closed-loop flutter was not encountered. The analytical results indicate a 34% increase.

The effective operation of the flutter suppression system is shown by the oscillograph trace of model response presented in Fig. 7. A typical time history of a bending strain gage with time increasing from left to right is shown in the figure. Open-loop flutter is shown on the left side, and closed-loop operation is shown on the right side. Note the increase in oscillatory amplitude until flutter begins. When the flutter suppression system is turned on (indicated by the dashed line in the figure), its effect is felt almost immediately and the oscillatory flutter motion rapidly damped. The degree of confidence in the closed-loop system was such that whenever open-loop flutter was encountered, the active control loop was closed to suppress the flutter motion. Or stating it another way, the flutter suppression system was literally used as a "flutter stopper."

To evaluate the active control system at other Mach numbers, Control Law C was both analytically and experimentally studied from $M=0.6$ to $M=0.9$. The results obtained are presented in Fig. 8 in terms of the variation of flutter-speed-index parameter with Mach number. The experimentally measured open-loop flutter boundary and the closed-loop no-flutter points for each Mach number are presented. At $M=0.8$ a 9.4% increase in flutter-speed-index (20% in dynamic pressure) is shown. Unfortunately, at this point the model was damaged due to saturation of the closed-loop system because of limited available actuator angles ($\pm 9°$). Saturation caused the analog computer amplifiers to overload and forced the control surface to go hard against its stop resulting in open-loop flutter. The model was repaired and tested at Mach numbers 0.7 and 0.6. A modest increase in flutter-speed-index of 5.7% (12% in dynamic pressure) was demonstrated at these two Mach numbers.

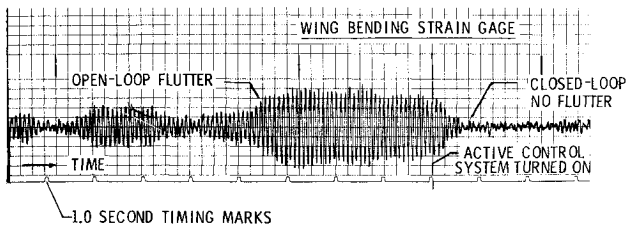

Fig. 7 Time history trace showing the effective operation of an active control flutter suppression system.

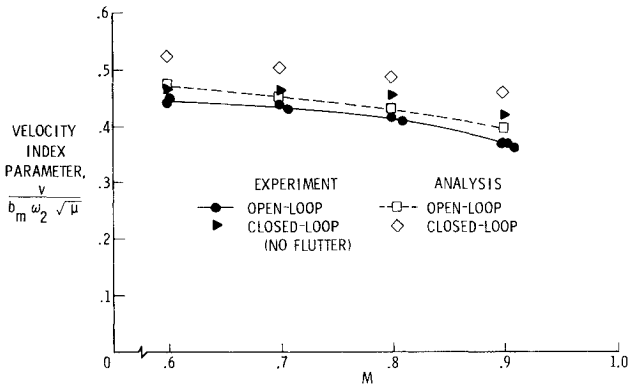

Fig. 8 Measured and calculated variation of flutter velocity index paramter with Mach number.

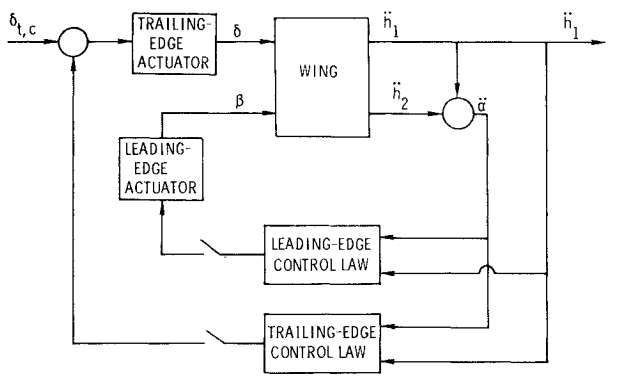

Fig. 9 Simplified diagram of flutter-suppression system.

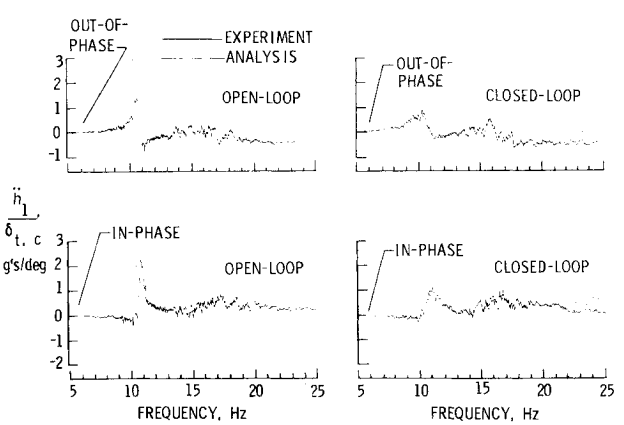

Fig. 10 A comparison of measured and calculated forced response of model to trailing-edge-control excitation at Mach number 0.9 and dynamic pressure of 5.03 kN/m^2.

A comparison of calculated and experimental results (Control Law C) is also presented in Fig. 8. The calcuations for the open-loop system show reasonable agreement at all Mach numbers.

Subcritical Response

To explore fully the behavior of the model below the flutter boundary and to assess the value of the calculations for predicting model response data, a forced response technique was used throughout these studies. The technique (described in Ref. 9) involves measuring the forced response of the model to a sinusoidal input generated by the trailing-edge control surface as indicated in Fig. 9. A measure of the damping in the desired flutter mode can be obtained for both open- and closed-loop operation if the transfer function relating the forced response to the command input signal ($\ddot{h}_1/\delta_{t,c}$) is determined as a function of frequency. During the wind-tunnel test an electronic signal analyzer was used to determine the in-phase and out-of-phase components of the response $\ddot{h}_1$ with respect to the trailing-edge command signal ($\delta_{t,c}$). Figure 10 presents a typical plot of this response at a Mach number of 0.9 and a dynamic pressure of 5.027 kN/m^2. The curves on the left side of this figure represent the model response for open-loop operation, and the curves on the right side represent the model response for closed-loop operation. A qualitative measure of the effect of active controls in reducing the forced response of the system is evident form Fig. 10. Also shown on Fig. 10 is a comparison of measured and calculated model response data. The analytical and experimental in-phase results are in good agreement. The agreement for the out-of-phase data is not as good, but the analysis does predict well the general behavior of this response.

Conclusions

A wind-tunnel study used to evaluate active control of flutter suppression has been described. A flutter-suppression method based on an aerodynamic-energy criterion has been described, and some results of the application of this method to a simplified delta-wing model are presented. Three different control laws were investigated. The first two used both leading- and trailing-edge control surfaces, whereas the third used a trailing-edge control surface alone. For this model study at a Mach number of 0.9 an increase in dynamic pressure of 22% has been achieved through the use of leading- and trailing-edge controls, and an increase in dynamic pressure of 30% has been achieved through the use of a trailing-edge control. Analytical calculations have been compared with experiment and indicate reasonable agreement.

References

[1] Nissim, E., "Flutter Suppression Using Active Controls Based on the Concept of Aerodynamic Energy," TN D-6199, 1971, NASA.

[2] Rainey, A. G., Ruhlin, C. L., and Sandford, M. C., "Active Control of Aeroelastic Response," Stability and Control, AGARD CP-119, 1972, pp. 16-1-16-5.

[3] Abel, I. and Sandford, M. C., "Status of Two Studies on Active Control of Aeroelastic Response," TM X-2909, Sept. 1973, NASA.

[4] Hunt, G. L. and Walberg, G. D., "Calculated Mode Shapes and Pressure Distributions at Flutter for a Highly Tapered Horizontal Tail in Subsonic Flow," TN D-1008, 1962, NASA.

[5] Garrick, I. E., "Perspectives in Aeroelasticity," *Israel Journal of Technology*, Vol. 10, No. 1-2, 1972, pp. 1-22.

[6] Bergmann, G. E. and Sevart, F. D., "Design and Evaluation of Miniature Control Surface Actuation Systems for Aeroelastic Models," AIAA Paper 73-323, Williamsburg, Va., 1973.

[7] Abel, Irving, "A Wind-Tunnel Evaluation of Analytical Techniques for Predicting Static Stability and Control Characteristics of Flexible Aircraft," TN D-6656, 1972, NASA.

[8] Albano, E. and Rodden, W. P., "A Doublet-Lattice Method for Calculating Lift Distributions on Oscillating Surfaces in Subsonic Flows," *AIAA Journal*, Vol. 7, No. 2, Feb. 1969, pp. 279-285.

[9] Keller, A. C., "Vector Component Techniques: A Modern Way to Measure Modes," *Sound and Vibration*, Vol. 3, No. 3, March 1969, pp. 18-26.